

Contents lists available at ScienceDirect

Catena

journal homepage: www.elsevier.com/locate/catena





Bridging structural and functional hydrological connectivity in dryland ecosystems

Octavia Crompton a,b,*, Gabriel Katul b, Dana A Lapides d,c, Sally E Thompson e

- ^a USDA ARS Hydrology and Remote Sensing Lab, USA
- ^b Department of Civil and Environmental Engineering, Duke University, USA
- ^c Pacific Southwest Research Station, USDA Forest Service, USA
- ^d Department of Geography, Simon Fraser University, Canada
- e Department of Civil and Environmental Engineering, University of Western Australia, Australia

ARTICLE INFO

Keywords: Connectivity Drylands Vegetation patterns Runoff Thresholds

ABSTRACT

On dryland hillslopes, vegetation water availability is often subsidized by the redistribution of rainfall runoff from bare soil (sources) to vegetation patches (sinks). In regions where rainfall volumes are too low to support spatially continuous plant growth, such functional connectivity between bare soil and vegetated areas enables the establishment and persistence of dryland ecosystems. Increasing the connectivity within bare soil areas can intensify runoff and increase water losses from hillslopes, disrupting this redistribution and reducing the water available to sustain ecosystem function. Inferring functional connectivity (from bare to vegetated, or within bare areas) from structural landscape features is an attractive approach to enable rapid, scalable characterization of dryland ecosystem function from remote observations. Such inference, however, would rely on metrics of structural connectivity, which describe the contiguity of bare soil areas. Several studies have observed non-stationarity in the relations between functional and structural connectivity metrics as rainfall conditions vary. Consequently, the suitability of using structural connectivity to provide a reliable proxy for functional connectivity remains uncertain and motivates the work here.

Relations between structural and functional connectivity metrics are established based on model simulations of rainfall-runoff on hillslopes with varying soil properties and vegetation patterns. These relations vary between two hydrologic limits – a 'local' (patch-scale) limit, in which functional connectivity is related to structural connectivity, and a 'global' (hillslope-scale) limit, in which functional connectivity is most related to the hillslope vegetation fraction regardless of the structural connectivity of bare soil areas. The transition between these limits within the simulations depends on rainfall intensity and duration, and soil permeability. While the local limit may strengthen positive feedbacks between vegetation and water availability, the implications of these limits for dryland functioning need further exploration, particularly considering the timescale separation between storm runoff production and vegetation growth.

1. Introduction

Drylands, water-limited regions with arid, semiarid, and dry subhumid climates, experience limited and sporadic rainfall (Reynolds et al., 2007; Maestre et al., 2012), which is generally insufficient to support continuous plant cover. Therefore, dryland vegetation often grows in patches surrounded by areas of bare soil. Vegetation patches may be randomly distributed or spatially organized into banded or patterned formations (Puigdefábregas, 2005; Penny et al., 2013). Bare areas and vegetated sites interact, forming connected sources and sinks for water, sediments, seeds, and nutrients (Noy-Meir, 1979; Schlesinger et al., 1990; Harman et al., 2014; Thompson et al., 2014). The mobilization, transport, and deposition of resources on the landscape are closely tied to vegetation spatial pattern: vegetation cover increases soil infiltration capacity and surface roughness (Dunkerley, 2002; Thompson et al., 2010a), such that vegetation patches can act as sinks for sediments and water (Ludwig et al., 1996; Cammeraat, 2004; Arnau-Rosalén et al., 2008). Overland flow generation is a primary transport mechanism linking sources and sinks in drylands (Okin et al., 2009; Okin et al., 2015). Overland flow transports water and nutrients from bare soil

^{*} Corresponding author at: USDA ARS Hydrology and Remote Sensing Lab, USA. *E-mail address:* octavia.crompton@usda.gov (O. Crompton).

to vegetated areas, augmenting plant water supply and creating a positive feedback between vegetation growth and plant-available resources (Thompson et al., 2011; Assouline et al., 2015). This positive feedback means that spatial patterns of vegetation provide a visible indicator of how runoff run-on processes 'play out' in space, and thus of ecosystem function (D'Odorico et al., 2006; Kéfi et al., 2007). However, interpreting observations of vegetation spatial distribution in terms of hillslope-scale ecosystem and hydrological processes remains elusive (but see e.g., Thompson and Katul, 2011). 'Connectivity' - a measure of landscape transport of water and sediments between locations and across scales (Turnbull et al., 2008; Wainwright et al., 2011) - has been proposed as a framework to interpret the relations between spatial structure and processes operating at hillslope to landscape scales (Bracken and Croke, 2007; Okin et al., 2015). Connectivity reflects the transfer of water or other materials between different sites in the landscape. Higher connectivity indicates more and longer pathways over which such transport occurs, while lower connectivity landscapes display shorter transport lengthscales (Okin et al., 2015). For example, when considering hydrologic connectivity, a lower connectivity landscape would tend to store water, solutes and sediments locally (resourceconserving). Conversely, a highly-connected landscape would tend to facilitate the large-scale transport and export of water (resource-shedding) (Okin et al., 2015; Saco and Moreno-de las Heras, 2013).

Changes in hydrologic connectivity (Turnbull et al., 2008) may coincide with threshold-like changes from healthy to degraded states documented in drylands worldwide (e.g., Anderies et al., 2002; Gibbens et al., 2005; Gao et al., 2011). One hypothesis for this behavior is that increasing hydrologic connectivity increases resource shedding from hillslopes, accelerating vegetation mortality (Mayor et al., 2019; Saco et al., 2020). Higher plant mortality would reduce vegetation cover, further increasing hydrologic connectivity of bare soil areas and concomitant resource loss (Okin et al., 2009). However, the connections between connectivity, productivity, and water stress within dryland ecosystems are not straightforward, particularly in spatially or ecologically complex ecosystems (Kéfi et al., 2022). In part, this is because measuring connectivity is inherently difficult and perhaps context-specific.

Measures of hydrologic connectivity attempt to link morphological features of the land surface, such as vegetation and topographic structure, to their hydrological responses (Ludwig et al., 2007b; Ludwig et al., 2007b; Mayor et al., 2008). Broadly, two approaches are used to consider the connectivity of a landscape - structural and functional (Bracken and Croke, 2007; Bracken et al., 2013). Structural connectivity measures describe connectivity based on analyses of landscape topography, microtopography, and vegetation pattern (Bracken and Croke, 2007; Ludwig et al., 2007b), whereas functional connectivity metrics describe the realized properties of resource mobilization, transport, and deposition (Bracken et al., 2013; Reaney et al., 2014; Cantón et al., 2011). These realized properties reflect the dynamic interactions between structural features of a landscape - such as topography and vegetation pattern - and dynamical properties, such as rainfall intensity/duration and soil permeability. These interactions can produce variable hydrologic responses for fixed structural properties, as reported in field (Mayor et al., 2009; Magliano et al., 2015; Rodríguez-Caballero et al., 2014) and modeling results (Crompton et al., 2019). This variability complicates the correspondence between structural and functional connectivity since a single structure can produce many functional responses. For example, recent studies have observed non-stationary relations between functional and structural connectivity metrics under varying rainfall and antecedent soil moisture conditions (Turnbull and Wainwright, 2019; Moreno-De-Las-Heras et al., 2020). These nonstationary relations are expected given the complexity of flow hydraulics on patchily vegetated dryland hillslopes (Smith et al., 2007; Dunkerley, 2003), and continue to challenge efforts to infer ecosystem function from observed vegetation patterns.

Nonetheless, structural connectivity measures are appealing due to

their suitability for remote sensing assessments, which can readily identify the spatial distributions of vegetated and bare soil areas and be applied at large, management-relevant scales (e.g., Mander et al., 2017; Rodríguez et al., 2018). The structural connectivity between mapped bare soil areas can then be quantified with metrics such as the flowlength index (FL), which measures the accumulated length of potential runoff pathways, considering vegetation pattern and topography (Mayor et al., 2009; Liu et al., 2013; Okin et al., 2015). Such structural metrics can have functional meaning - for example, a remote sensing analysis of banded Mulga landscapes in Australia (data shown in Fig. 1, Saco et al., 2020) identified a breakpoint in ecosystem function for vegetation cover of 30%, below which the flowlength greatly increased and the Mulga ecosystem was hypothesized to shift from resource-conserving to resource-shedding. More generally, structural connectivity metrics such as FL display geometrically-imposed nonlinear sensitivities to changing vegetation cover fraction (see Fig. 1). This type of nonlinearity has been proposed as a mechanism for abrupt ecosystem shifts in drylands (e.g., Okin et al., 2015; Rodríguez et al., 2018; Saco et al., 2020). However, functional connectivity may behave differently from structural connectivity, depending on the rainfall regime, soil properties, and hillslope

Thus, while structural connectivity is straightforward to quantify, it does not always reflect functional connectivity. Conversely, functional connectivity is difficult to observe and quantify, but is more likely to be directly related to ecosystem outcomes than structural connectivity. Given that structural connectivity metrics are typically the only metrics that can be applied at large scale to support the management of drylands, methods to relate functional and structural connectivity metrics would be valuable. Specifically, determining when structural methods do or do not reflect functional connectivity would inform the appropriate use of structural connectivity to predict ecosystem outcomes and trajectories.

To investigate the correspondence between functional and structural connectivities, we use virtual experiments to explore the rainfall and landscape conditions under which a widely-used structural connectivity metric – the flowlength index, *FL* (Mayor et al., 2008) – reliably indicates functional connectivity. Virtual experiments allow the source-sink behavior of runoff to be mathematically modeled across a range of rainfall, vegetation, and landscape characteristics (Fatichi et al., 2016) so that the influences of these factors on runoff connectivity can be isolated and separately quantified.

As an organizing framework, we address two related research questions:

- How is the relation between vegetation cover fraction and functional connectivity altered with changing rainfall conditions? How does it compare to the relation between vegetation cover and structural connectivity?
- Under what rainfall conditions is structural connectivity as measured by the flowlength index – a robust indicator of functional connectivity?

2. Methods

2.1. SVE model

The virtual experiments performed here use an open-source physics-based model for shallow two-dimensional surface flows (Full Shallow Water equations for Overland Flow, FullSWOF 2D; Delestre et al., 2014), adapted to represent rainfall-driven runoff on patchily-vegetated dryland hillslopes. Model simulations comprise discrete storm events. The model domain is a hillslope with a constant slope S_o , length W_x and width W_y , where x increases in the downslope direction from 0 at the divide to W_x at the outlet. The hillslope consists of a mosaic of bare soil areas and interspersed vegetation patches (see Section 2.2). The presence/absence of vegetation is used to prescribe the permeability and

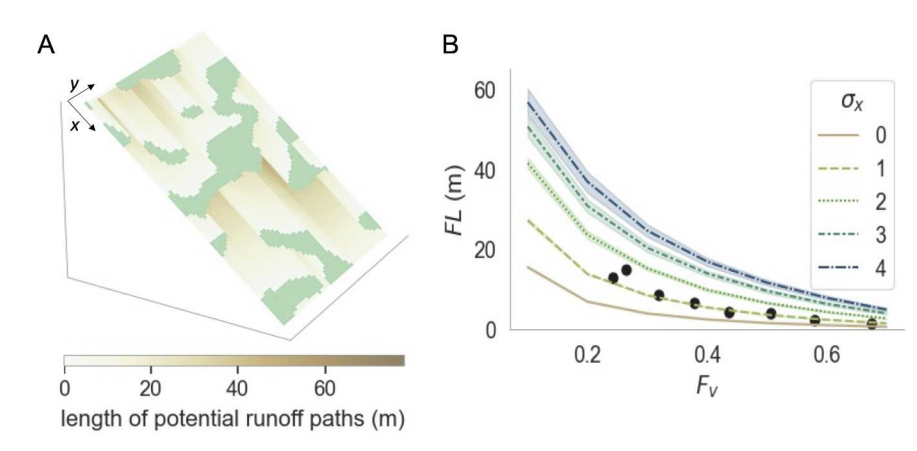


Fig. 1. (A) Illustration of how the flowlength index (FL) is computed as the average length of all the potential runoff pathways in the hillslope area. Brown shading indicates the potential flowpath lengths along bare-soil areas, and the vegetation is shown in green (flowpath lengths = 0). Hillslope dimensions are 200 m in length by 50 m in width. (B) FL increases nonlinearly as vegetation fraction (F_{ν}) declines, regardless of the vegetation patch lengthscale (σ_x). For a plausibility check, markers show published data from the banded Mulga example (Saco et al., 2020).

surface roughness (similar to previous modeling, field and remote sensing studies, e.g., Imeson and Prinsen, 2004; Rodríguez et al., 2018; Moreno-De-Las-Heras et al., 2020). Rainfall is represented by a spatially uniform and temporally-invariant intensity p [L/T] for a storm duration t_R [T]. Overland flow is initiated at a given point if p exceeds the local infiltration capacity.

Such flows are conventionally represented by the Saint Venant Equations (SVE), also known as the shallow water equations (Brutsaert, 2005). These equations combine the continuity equation with conservation of momentum to describe water depth and depth-averaged velocity in space and time. While the simulations use the full 2D form of the equations, their one-dimensional form is shown below for illustration:

$$\frac{\partial h}{\partial t} + \frac{\partial (hU)}{\partial x} = p - i \tag{1}$$

$$\frac{\partial U}{\partial t} + U \frac{\partial U}{\partial x} + g \left[\frac{\partial h}{\partial x} - (S_o - S_f) \right] = 0.$$
 (2)

Here, h is the water depth at location x and time t, U is the depth-averaged velocity, S_o and S_f are the local bed- and friction- slopes, and g is the gravitational acceleration. The imbalance between rainfall p and infiltration i represents a runoff-generation term that can vary with x and t.

The SVE do not form a closed system of equations as they offer two equations (conservation of mass and momentum along the longitudinal direction) in 3-unknowns $(h, U, \text{ and } S_f)$. A closure model in the form of a resistance formulation must be specified to represent the effects of bed and other shear stresses (e.g., the presence of obstructions) on S_f . The general form of this closure model is given by:

$$S_f = (R_h F r)^2, \tag{3}$$

where R_h is a dimensionless resistance factor, and $Fr = U(gh)^{-1/2}$ is the local Froude number measuring how fast pressure disturbances travel $(gh)^{-1/2}$ in relation to inertia (i.e. U). R_h is determined by the vegetation and soil properties, and consequently differs between vegetated and bare soil areas. Both surface types can be accommodated in a single formulation given by (James et al., 2004):

$$R_h^2 = \frac{\frac{f}{8} + C_{d_2}^{\frac{1}{2}}hDN}{1 - \phi_{..}},\tag{4}$$

where f is the Darcy–Weisbach friction factor for the soil surface, ϕ_{ν} is the areal stem density (the volume fraction occupied by the vegetation), D is the stem diameter, $N=4\phi_{\nu}(\pi D^2)^{-1}$ is the number of stems per unit ground area, and C_d is a vegetation drag coefficient, which depends on the vegetation characteristics and U. In bare soil areas $\phi_{\nu}=0$ so that

 $R_h^2 = f/8$. In vegetated patches, both stem drag and ground friction can be significant, with stem drag dominating R_h for higher h values and ground friction dominating for lower h values.

To represent dryland grasses or shrubs, a 'cylinder array' formulation for the drag coefficient is employed (Cheng and Nguyen, 2011), described in supporting information Text S1. Briefly, C_d is parameterized as a function of U and a vegetation-related Reynolds number $Re_{\nu} = Ur_{\nu}/\nu$, where ν is the kinematic viscosity and r_{ν} is a vegetation related hydraulic radius given by

$$r_{v} = D\left(\frac{\pi}{4} \frac{1 - \phi_{v}}{\phi_{v}}\right). \tag{5}$$

 ϕ_v and D jointly control r_v , and thus Re_v , forming one functional group. To vary Re_v , only ϕ_v is varied in the SVE simulations for simplicity, and D is held constant.

We selected a modified laminar formulation for f, anticipating low bulk Reynolds numbers ($Re = Uh/\nu < 3000$) for the simulated p and hillslope lengthscales (see Table 1):

$$f = \begin{cases} 24(Re^{-1}) & \text{when } Re < 48\\ 0.5 & \text{otherwise.} \end{cases}$$
 (6)

This formulation for *f* recovers the Poiseuille solution for low *Re* in wide channels. Its acceptable performance at low *Re* (i.e., when the viscous sublayer exceeds the local roughness originating from soil grains and microtopography) has been verified in flume experiments described elsewhere (Kirstetter et al., 2016).

A criterion for the use of the SVE is that the flow is subcritical

Table 1 Parameters used in the 2-D SVE model simulations. Where multiple entries are listed, all possible combinations of these parameters were run in simulations (cases with p=1 cm/hr and $K_b=1.5$ cm/hr were not included because no runoff is generated).

Variable	Symbol	Values			
Hillslope topography					
Slope gradient (%)	S_o	0.5, 5%			
Domain size	W_x, W_y	$200~m\times50~m$			
Storm and soil parameters					
Storm duration	t_R	10, 30, 60 min			
Rainfall intensity	p	1, 3, 5, 7 cm/hr			
Hydraulic conductivity (vegetated)	K_{ν}	3, 7 cm/hr			
Hydraulic conductivity (bare soil)	K_b	0.2, 1.5 cm/hr			
Vegetation pattern parameters					
Vegetation fraction	F_{ν}	0.05, 0.1, 0.2, 0.3, 0.4, 0.5			
Vegetation patch lengthscale	$\sigma_{ m y}$	2, 3, 4			
Vegetation patch anisotropy	σ_{x}/σ_{y}	1, 3			
Flow resistance parameters					
Within-patch stem density	$\phi_{ u}$	0.15			
Stem diameter	D	5 mm			

(Fr < 1) at all times and locations, which places an upper limit on the mean hillslope gradients simulated. Higher slope gradients produce supercritical flow, which transitions to subcritical flow via a hydraulic jump. Hydraulic jumps do not abide by the closure scheme for S_f in Eq. 3. For this reason, conditions promoting their occurrences (i.e. supercritical to subcritical) are avoided.

Infiltration rates in the model, like roughness, are determined by whether the surface cover is bare or vegetated. Infiltration rates are assumed to be low in bare soil areas due to the formation of physical and biological surface crusts (Belnap, 2006; Bautista et al., 2007; Assouline, 2004; Assouline et al., 2015) that reduce surface-water infiltration (Belnap, 2006; Assouline, 2004), and higher under vegetation cover due to root activity and protection of the soil surface against rain-splash (Thompson et al., 2010b). While the modeling framework can accommodate variability of the infiltration capacity with antecedent wetness, we simplify the model scenarios to be examined by assuming that infiltration is steady (wet antecedent conditions in all cases). The saturated hydraulic conductivities in vegetation patches, $K_{\nu} = 3$ and 7 cm/hr, are representative values selected from field studies (e.g., Vásquez-Méndez et al., 2010; Garcia-Estringana et al., 2010, and see Table S2).

For the bare sites, the selected values include a limiting case in which the soil is nearly impermeable ($K_b=0.2~{\rm cm/hr}$, based on observed rates of infiltration into crusted soils, Valentin and Casenave, 1992; Šimunek et al., 1998; Assouline et al., 2015), and one based on K_v/K_b ratios reported in the literature ($K_b=1.5~{\rm cm/hr}$, see Table S2). The smaller value (0.2 cm/hr) is also realistic given that K_b can be considered an effective parameter that represents the influence of surface crusts, including those that dynamically form due to the kinetic energy of raindrops on unprotected soils (Mügler et al., 2019). It is to be noted that infiltrometer measurements do not reflect crusted conditions dynamically formed by the kinetic energy in raindrops.

The influence of vegetation on runoff connectivity is expected to decrease as the difference between infiltration properties in vegetated and unvegetated areas decreases, and in the limit that $K_b=K_\nu$ would arise entirely from second-order effects of surface roughness. To focus on the influence of vegetation, the manuscript figures show model predictions with $K_b=0.2$ cm/hr. The results with $K_b=1.5$ cm/hr are qualitatively similar (see SI Figures S5-S8), with the principal difference being that the influence of vegetation is diminished (as expected, given that the difference in surface properties is also smaller).

Because the modeled land surface is permeable, any fluid element has a finite probability of either being advected down-gradient, or being infiltrated into the soil at any point in time. These probabilities vary depending on the flow depth and infiltration rate at the location of the fluid element. Because velocity and infiltration rate vary through space, the probable path length traversed by a fluid element differs across the hillslope. These path lengths represent the lengthscales of source-sink transport. To understand these lengthscales, we simulated the x-ytrajectories of massless tracers advected in the depth-averaged flow field. For each SVE simulation, 2000 tracers were initialized at random positions on the hillslope and random times ranging from 0 to t_R (the storm duration). The trajectory of each tracer was then computed assuming advection by the 2-D flow, forming a pathline from its initial location. At each timestep (dt = 60 s), a given tracer infiltrates with probability $i \cdot dt/(h' + p \cdot dt)$, where *i* is the local infiltration rate (K_v or K_b) and h' is flow depth at the tracer's location. To ensure that 2000 tracers were adequate to represent runoff pathways, we confirmed that the hillslope runoff coefficient (cumulative hillslope discharge as a fraction of cumulative hillslope rainfall input) calculated from the SVE, and the fraction of tracers that escape the hillslope differed by less than 5%.

Simulations were then run for storms with the rainfall conditions summarized in Table 1, for 36 vegetation patterns (see Section 2.2). For each combination of vegetation pattern and rainfall, the SVE model was used to simulate runoff and the transport of massless particle tracers in the flow. The simulation results were used to define functional

connectivity across storm and landscape conditions (see Section 2.3).

2.2. Vegetation patterns and structural connectivity

The SVE were applied to a set of landscapes with different vegetation patterns. These patterns were generated from arrays of uniformly-distributed random numbers between 0 and 1, which were binarized to obtain a given vegetation cover fraction, F_{ν} , by adjusting the threshold value used to binarize the array. The characteristic patch length-scale was adjusted by applying a two-dimensional Gaussian filter prior to binarizing. This Gaussian filter uses a kernel defined by standard deviations in the x and y directions (σ_x along slope and σ_y across slope), which then set the length-scale of the vegetation patches in each direction. Because dryland vegetation often forms spatially-organized vegetation patterns (Noy-Meir, 1979), we adjusted the ratio of σ_y/σ_x to generate isotropic patterns ($\sigma_y = \sigma_x$) and anisotropic patterns that extend along the hillslope contour ($\sigma_y/\sigma_x > 1$). Fig. 2 illustrates several vegetation patterns generated with this approach, with sample anisotropic patterns included in supporting information Figure S2.

We generated 36 unique vegetation patterns by varying the following: (i) vegetation cover fraction F_{ν} , (ii) patch-length scale σ_{x} , and (iii) anisotropy σ_{y}/σ_{x} (see parameters listed in Table 1). The tested F_{ν} ranged from 5 to 50%. This range focuses on lower F_{ν} values, for which previous studies have identified greater sensitivity of hydrologic connectivity to changing vegetation cover (Gao et al., 2011; Mayor et al., 2019).

We surveyed literature regarding structural connectivity metrics (see supporting information Text S2). Not all structural connectivity metrics can be applied to describe the connectivity of mosaic-type landscapes. However, the flowlength index *FL* (Mayor et al., 2009), the directional leakiness index (*DLI*) and other variations of the leakiness index (Ludwig et al., 2002; Ludwig et al., 2007a), cohesion (Schumaker, 1996), the adjacency matrix (Masselink et al., 2017), and contagion metrics (Li and Reynolds, 1994) can be applied. Among these metrics, only *FL* and *DLI* can account for a slope gradient.

The flowlength index is the more commonly used connectivity metric of FL and DLI (see Table S1 and Figure S1), and increases in FL appear to be related to desertification in some studies (Saco et al., 2020). Additionally, DLI is highly correlated to FL (see SI Figure S3). Therefore, we restrict the focus here on FL as the structural connectivity metric (Muñoz-Robles et al., 2013; Wu et al., 2016; Rodríguez et al., 2018).

The flowlength index is computed as a function of the *potential* runoff path lengths, which depend on flowlines determined by the landscape

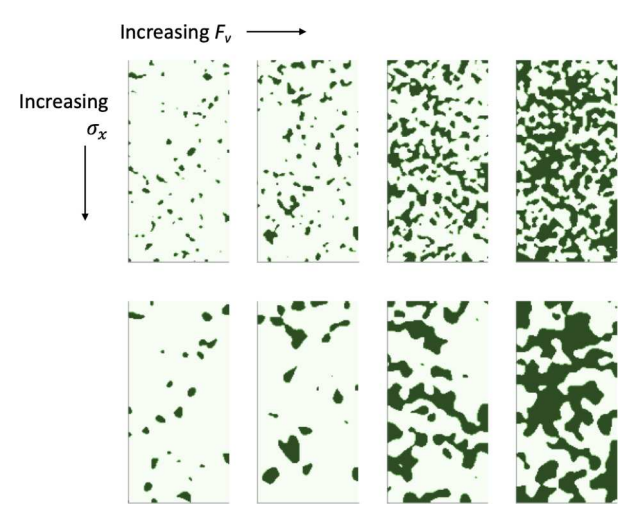


Fig. 2. Vegetation patterns generated for varying vegetation cover fractions, F_{ν} (columns), and for short and long vegetation patch lengthscales, σ_{x} (rows). Green indicates vegetation, and white indicates bare soil areas.

topography and the vegetation pattern (as described in Mayor et al., 2008). The potential runoff path lengths are defined, for each cell in the domain, as the length of a flowline starting at that cell, following the path of steepest descent and terminating either at the first vegetated cell reached, or the hillslope outlet (see Fig. 1 for illustration). FL is then computed as the average length of all the potential runoff path lengths in the hillslope. The resulting index varies nonlinearly with F_{ν} , as shown in Fig. 1B.

For the situation simulated here, where the topography of the hill-slope is planar (no curvature) and where microtopographic lengthscales are assumed small relative to those of bare soil areas, the calculation of flowlength simplifies to the distance from any bare soil pixel to the nearest downslope vegetated pixel (or outflow), as illustrated in Fig. 1A for a given vegetation pattern. No information about rainfall, infiltration capacity, or velocity variations are needed to calculate FL. Remote sensing analyses of FL often closely approximate this assumption even on topographically complex slopes, as detailed topographic information at < 30 m resolution is typically not available (see Fig. 3).

2.3. Functional connectivity metrics

Functional connectivity metrics are those that can represent the *realized* as opposed to *potential* flow redistribution. The runoff coefficient *C*, defined as the fraction of incident rainfall volume that is routed to the outlet and exported from the hillslope over a given time period, is one way of representing this realized redistribution. Increasing *C* implies an increase in the proportion of rainfall lost from the hillslope, providing a global functional connectivity metric (Mayor et al., 2019).

However, as a metric C is necessarily lumped at hillslope scales. That is, C misses the transfer of runoff from bare-soil areas to vegetation patches, i.e., local connectivity. To distinguish hillslope-scale resource losses from local subsidies to vegetation, a measure of within-slope functional connectivity is needed as well.

Previous approaches to defining functional connectivity within hillslopes focused on metrics such as the length of connected runoff pathways (e.g., the length of dynamic, event-based transport pathways Turnbull and Wainwright, 2019). However, such metrics neglect the infiltration of runoff along these pathways. Where infiltration is significant, the connected runoff length could contain numerous source-sink pathways - i.e., paths along which a fluid element arrives as rainfall, advects, and then infiltrates. Quantifying these source-sink path lengths offers a way to characterize functional connectivity on heterogeneous hillslopes where connected runoff paths traverse locations of high infiltration capacity. Mathematically, such source-sink path lengths are also less likely to saturate to the length of the hillslope than metrics of connected runoff. Thus, source-sink path lengths may enable the characterization of differences in functional connectivity across a wider range of hillslope and storm conditions than simple runoff lengthscales. We used the behavior of the passive, infiltrating tracers in the model to define a source-sink connectivity metric, L_{infl} . This metric was computed as the mean distance traveled by the tracers before they infiltrated. The three measures of structural and functional connectivity – L_{esc} , L_{infl} and C

- are summarized in Table 2.

With these metrics, we addressed the first research question (RQ 1) by plotting the functional connectivity metrics against the vegetation cover fraction, grouping the data by rainfall, topographic and soil characteristics, in order to isolate (for each rainfall/landscape scenario) the vegetation's effect on functional connectivity (Section 3.1). The same approach was repeated in relating the flowlength index to the vegetation cover fraction. We then address RQ 2 by delineating – for each scenario – whether the flowlength index (embedding information about spatial pattern) versus the hillslope vegetation cover fraction (a bulk measure) is more closely related to the simulated functional connectivity.

3. Results

3.1. Relations between vegetation cover fraction and functional connectivity metrics

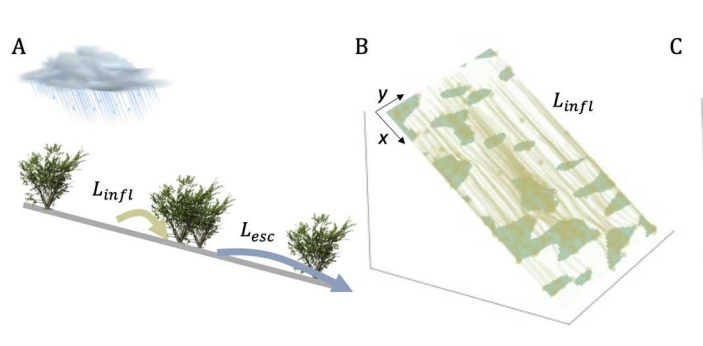
Fig. 4 features the variation in the global functional connectivity metric (i.e., C) with increasing vegetation fractional cover for all simulated storm intensities and duration. Across all simulated variations in storm intensity and duration, soil permeability, and vegetation pattern, the runoff coefficient C declines with increasing vegetation fraction F_{ν} . However, the nature of this decline varies with the factors that affect runoff production. Where runoff production potential is lower (i.e., shorter, lower intensity storms or higher infiltration rates), the C- F_{ν} relation is nonlinear. Where runoff production potential is higher - for longer, higher intensity storms and lower infiltration rates, C is linearly related to F_{ν} . The transition from the nonlinear C- F_{ν} regime to the linear regime is also sensitive to S_{o} , with linear behavior arising on steeper (5%) slope angles (see SI Figure S9).

The effect of the details of the vegetation pattern on the results can be seen in the vertical spread of points representing the modeled C for each simulation (for a given F_v , p and K_s). This spread of points arises from varying σ_x and σ_y/σ_x for a given F_v . The vertical scatter is greatest for low F_v and for conditions with lower runoff production potential – i.e., shorter, lower intensity storms and higher K_s .

A similar non-stationarity is seen in the relation between L_{infl} and F_{ν} ,

Table 2 Definitions of connectivity descriptors. Lengthscales L_{infl} and FL are normalized by the hillslope length W_x and vary from 0 to 1.

	-			
Variable	Symbol	Scale	Туре	Description
Flowlength	FL	Whole hillslope	Structural	Mean downslope extent of connected bare soil patches (Mayor et al., 2008).
Source-sink connectivity	L_{infl}	Within hillslope	Functional	Mean distance traveled by tracers that infiltrate.
Runoff coefficient	С	Whole hillslope	Functional	Fraction of rainfall that leaves the hillslope as runoff.



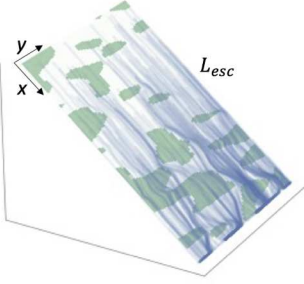


Fig. 3. (A) Definitional sketch of source-sink connectivity L_{infl} in yellow (tracers that infiltrate) and outlet connectivity L_{esc} in blue (tracers that escape). Panels B and C further illustrate the paths of tracers that infiltrate (B) and escape (C) for the simulation case with p=5 cm/hr, $t_R=60$ min, $F_V=0.3$, and $\sigma=4$. L_{infl} is defined as the average displacement of tracers that infiltrate, and L_{esc} as the average displacement of tracers that escape. L_{esc} is included here for concept clarification contrasting it to the definition of L_{infl} .

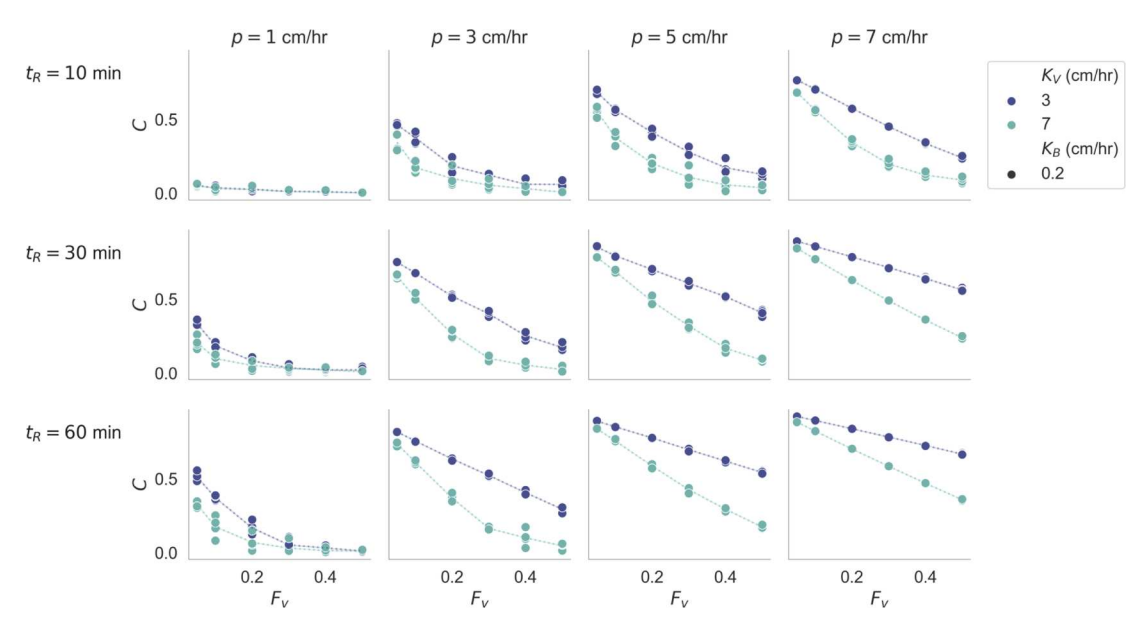


Fig. 4. Relating vegetation cover fraction F_V and runoff coefficient C across storm conditions, with each point summarizing one of the SVE simulations. Line colors indicate the saturated hydrologic conductivity in vegetated patches K_V . For a given F_V and K_V , markers show variation across vegetation patch lengthscales σ_X and anisotropies σ_Y/σ_X . The relation between F_V and C becomes increasingly linear with increasing storm intensity and duration (lower right). For low-intensity and short-duration storms, C increases nonlinearly with decreasing vegetation cover (upper left).

which is nonlinear for shorter, lower-intensity storms, and becomes progressively more linear as the storm duration and intensity increase (as shown in Fig. 5). The transition from nonlinear to linear is similarly sensitive to K_{ν} and S_{o} . Compared to the runoff coefficient, the relation between F_{ν} and L_{infl} shows more variation across the vegetation patterns (see greater vertical scatter in Fig. 5, for a given F_{ν} and K_{ν}). Again, the vertical scatter is greatest for short-duration storms, less intense rainfall, and lower K_{s} . Thus functional connectivity, whether measured globally (C) or within hillslopes (L_{infl}) appears to lose sensitivity to the details of the vegetation spatial pattern for a given F_{ν} when runoff production potential is high.

3.2. Conditions as to when structural connectivity relates to functional connectivity

The non-stationary relation between F_{ν} and functional connectivity metrics under different storm and soil conditions is likely related to the non-stationarity that exists between FL and functional connectivity metrics. For example, in Fig. 6, a *linear* relation emerges between FL and L_{infl} under conditions with low runoff production potential (low intensity, short duration storms), the same conditions under which F_{ν} and FL are nonlinearly related (compare lower left corners of Figs. 5 and 6). Under high runoff production potentials (high intensity, long duration), L_{infl} is linearly dependent on F_{ν} but weakly, and nonlinearly, related to

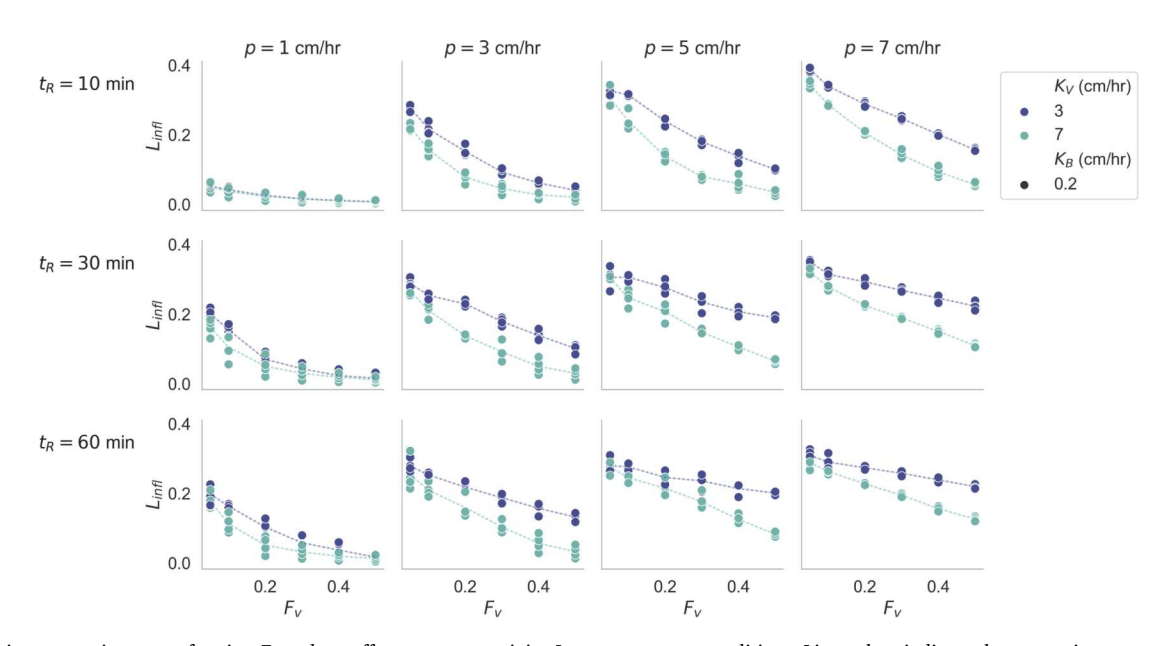


Fig. 5. Relating vegetation cover fraction F_{ν} and runoff run-on connectivity L_{infl} across storm conditions. Line colors indicate the vegetation saturated hydrologic conductivity K_{ν} . For a given F_{ν} and K_{ν} , markers show variation across vegetation patch lengthscales σ_{x} and anisotropies σ_{y}/σ_{x} . The relation between F_{ν} and L_{infl} becomes increasingly linear with increasing storm intensity and duration (lower right). For low-intensity and short-duration storms, L_{infl} increases nonlinearly with decreasing vegetation cover (upper left).

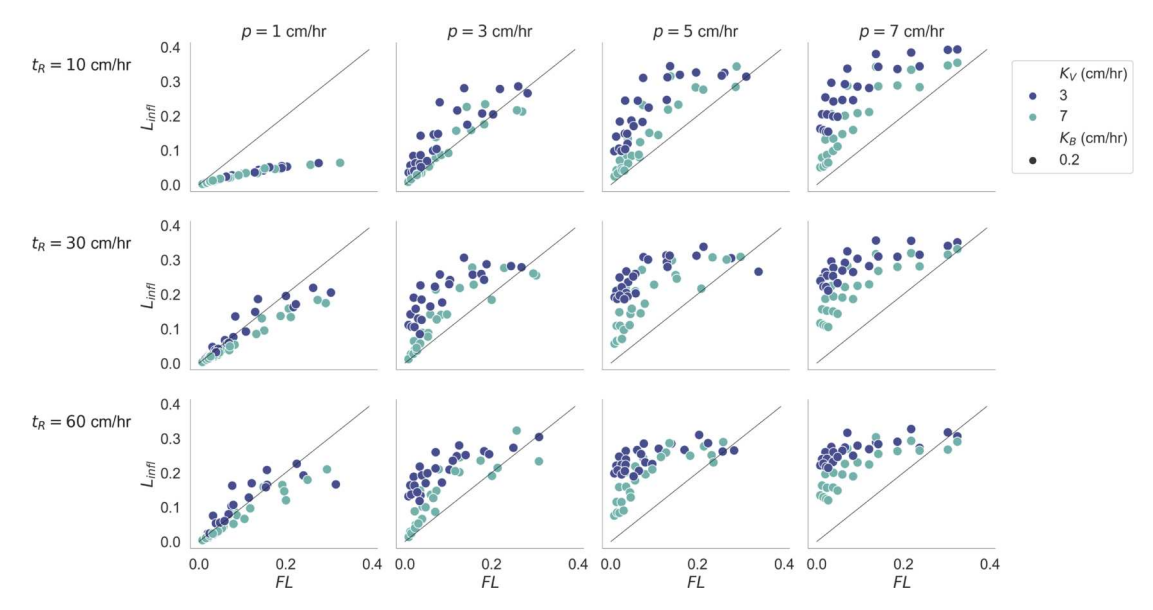


Fig. 6. Scatter plots relate flowlength FL (normalized by the hillslope length W_x) and source-sink connectivity L_{infl} across storm conditions. The two are linearly related for low rainfall intensities and short-duration events. The relation between FL and L_{infl} becomes less linear with increasing rainfall intensity and duration. Supporting information Figure S6 shows the case $K_b = 1.5$ cm/hr. Analogous figures, relating FL to C, are included in SI Figures S7 and S8 (corresponding to $K_b = 0.2$ and 1.5 cm/hr, respectively).

FL.

3.3. 'Global' and 'Local' limits

The non-stationary behavior observed in Section 3.1 of C and L_{infl} with respect to storm properties suggest two bounding limits of runoff connectivity – 'local' and 'global' – illustrated schematically in Fig. 7. In the local limit, low-intensity and short-duration rainfall results in lower runoff production, and lengthscales of functional connectivity that are comparable to or smaller than structural connectivity lengthscales (i.e., $L_{infl} \leq FL$). In this limit, runoff flowpaths are determined by structural controls such as vegetation patch lengthscales (Turnbull and Wainwright, 2019). Structural connectivity provides a close approximation of functional connectivity in this regime, such that C and L_{infl} can be predicted from structural connectivity indices (e.g. FL). In this regime, runoff mostly redistributes water and other resources within the hill-slope, functioning to conserve resources.

In the global limit, high-intensity, long-duration storms generate runoff with lengthscales exceeding those of vegetation patches (lower right corner in Fig. 6). The resulting high runoff connectivity promotes the export of resources from the hillslope. In this limit, the mean vegetation cover fraction provides a measure of hillslope-scale infiltration losses, such that runoff connectivity (as measured by L_{infl}) is sensitive to the mean vegetation cover fraction rather than the local spatial

organization of the vegetation.

To characterize the gradual transition between these limits, we regressed the functional connectivity metrics – C and L_{infl} – on F_{ν} for each combination of p, t_R and K_{ν} : for each $p/t_R/K_{\nu}$ scenario, N=48, corresponding to $6F_{\nu}\times 4\sigma_{x}\times 2\sigma_{y}/\sigma_{x}$ unique vegetation patterns. For a given scenario, the coefficient of determination (R^2) indicates the strength of the linear relation between F_{ν} and C (Fig. 8A) and and between F_{ν} and L_{infl} (Fig. 8B). The computed coefficients of determination – $R^2(F_{\nu},C)$ and $R^2(F_{\nu},L_{infl})$ – exclude any information about vegetation spatial pattern, providing a measure of how well variability in C and L_{infl} can be described from variability in vegetation fraction alone (assuming linear regression). In these panels, increasing $R^2(F_{\nu},C)$ and $R^2(F_{\nu},L_{infl})$ indicates that the landscape is approaching the global limit in which functional connectivity is strongly related to F_{ν} .

To further characterize the local-to-global transition, we regressed functional connectivity metrics on the flowlength FL for each scenario (Fig. 8, panels C and D). In this case, the coefficients of determination – $R^2(FL,C)$ and $R^2(FL,L_{infl})$ – describe the strength of the linear relations between structural and functional connectivity metrics, with higher values corresponding to the *local* limit. In these panels, as $R^2(FL,C)$ and $R^2(FL,L_{infl})$ decrease, this indicates that the landscape is approaching the global limit in which functional connectivity is weakly related to FL. All Fig. 8 subplots are shown as a function of $p-K_v$ on the horizontal axis,

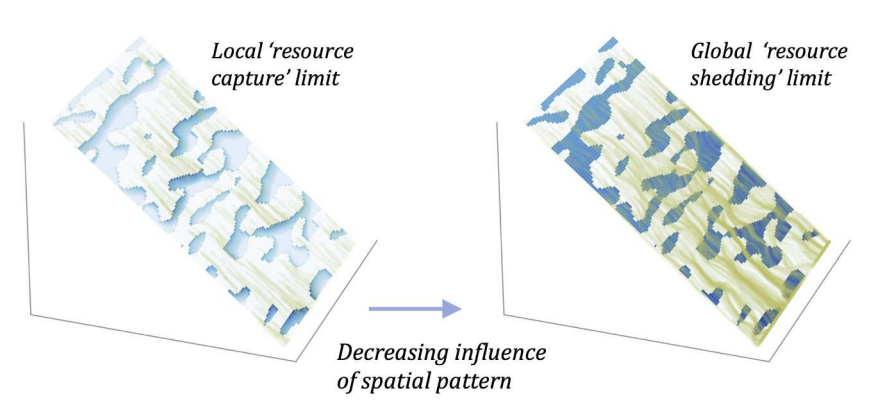


Fig. 7. Illustrating 'global' and 'local' limiting cases. In the local limit, functional connectivity lengthscales are comparable to or smaller than the structural connectivity lengthscales (i.e., $L_{infl} \le FL$), and runoff flowpaths are determined by structural controls. In the global limit, by contrast, runoff lengthscales exceed structural lengthscales, and runoff connectivity is more sensitive to the hillslope-mean vegetation cover fraction than its spatial organization. The 'local' limit is illustrated with the p=3 cm/hr, $t_R=10$ min simulation case, and the 'global' limit is illustrated with the p=7 cm/hr, $t_R=60$ min case (with $t_P=0.3$, $t_P=0$ cm/hr, $t_P=0.3$, $t_P=0$ min case).

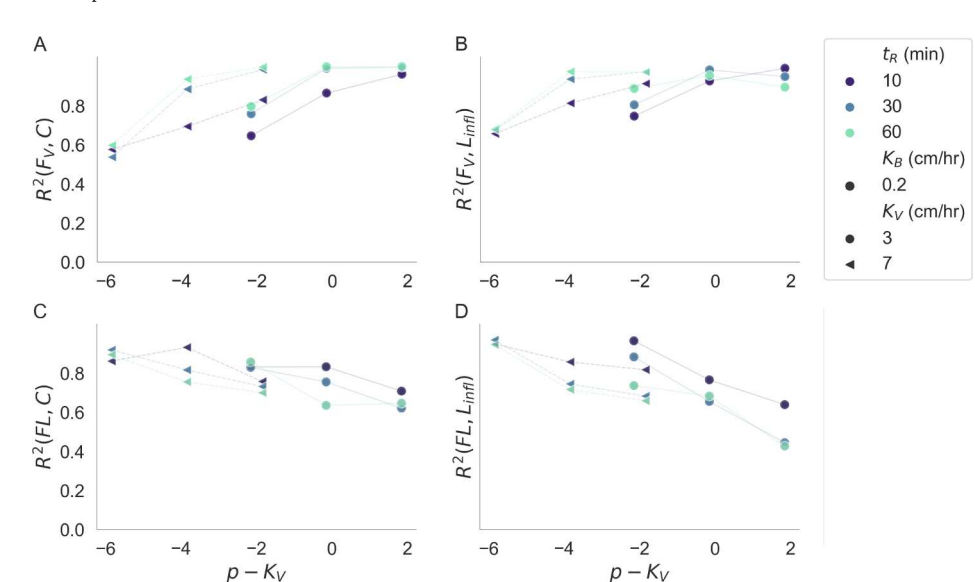


Fig. 8. Panels A and B show, for each combination of p, t_R and K_ν , the coefficients of determination (R^2) for the runoff coefficient C regressed on the vegetation cover fraction F_ν (panel A) and the source-sink connectivity L_{infl} regressed on F_ν (panel B), plotted against the rainfall intensity in excess of the infiltration capacity of vegetated areas, $p-K_\nu$. Marker colors show the storm duration t_R , and marker shapes show K_ν (the small horizontal offset between $K_\nu=3$ and 7 cm/hr is for visual clarity). Panels C and D analogously show the coefficients of determination for C regressed on the flowlength FL (panel C) and L_{infl} regressed on FL (panel D).

which is a measure of the strength of vegetation sinks in the landscape. As vegetation sinks become stronger (more negative), more water is captured locally, enhancing the importance of local effects over global.

In relating F_{ν} and C (Fig. 8A), smaller $R^2(F_{\nu},C)$ values for $p \ll K_{\nu}$ represent the local limit, where the relation between F_{ν} and C is nonlinear and scattered (lower left corner in Fig. 4). With increasing storm intensity, $R^2(F_{\nu},C)$ then increases towards 1.0 in the global limit, where C approaches a linear function of F_{ν} that is largely insensitive to the vegetation spatial pattern (upper right corner in Fig. 4). The dependence of this transition on the rainfall excess $(p-K_{\nu})$ depends on the storm duration t_R (marker color) and infiltration capacity of vegetated areas K_{ν} (marker shape). The global limit is approached for lower $p-K_{\nu}$ for longer storms than shorter storms. Similar trends can be seen in the correlation between F_{ν} and L_{infl} (Fig. 8B).

The lower row of Fig. 8 tells a consistent story: $R^2(FL,C)$ and $R^2(FL,L_{infl})$ values are large where $p \ll K_{\nu}$, and decrease with increasing p towards the global limit as the relative importance of spatial pattern decreases. As above, the dependence of this transition on $p-K_{\nu}$ depends on t_R and K_{ν} . For a given $p-K_{\nu}$, the flowlength index and functional connectivity metrics are more strongly correlated for lower $K_{\nu}-$ conditions where the vegetation patches are weaker sinks relative to rainfall intensity (compare $K_{\nu}=3$ and 7 cm/hr for simulation cases with $p-K_{\nu}=2$ cm/hr in Panels C and D).

To summarize, as $p-K_{\nu}$ and t_R increase, FL and C become increasingly decoupled (panel C), whereas F_{ν} and C become highly correlated (panel A). Similar trends can be seen for the source-sink connectivity: $R^2(FL, L_{infl})$ decreases with increasing $p-K_{\nu}$ and t_R (panel D), while $R^2(FL, C)$ increases. In both limits, functional connectivity is reasonably predicted by structural indices: F_{ν} in the global limit, and FL in the local limit.

4. Discussion

The study shows that functional connectivity reflects interactions between landscape structure and rainfall conditions at storm timescales. As storm intensity and duration increase, hydrologic outcomes become less sensitive to the spatial pattern of vegetation. If rainfall intensity p exceeds the infiltration capacity of vegetation patches K_{ν} , the source-sink connectivity lengthscales L_{infl} tend to exceed those of bare soil connectivity, so that in the case of the indices considered here, $L_{infl} > FL$. Conversely, if $p < K_{\nu}$ and runoff is generated in bare soil areas, structural connectivity provides a reasonable indicator of runoff connectivity. The transition between these limiting cases in parameter space – a transition

determining whether landscape structure indices are good predictors of functional connectivity – depends on the rainfall rate, the soil infiltration capacity in vegetated sites, and the hillslope gradient.

The local and global limiting cases have different implications for the ansatz that changes in runoff connectivity mediate abrupt changes in ecosystem function. In the global limit, when functional connectivity is driven by rainfall characteristics and vegetation fraction, changes in vegetation cover fraction F_{ν} produce linear changes in functional connectivity. However, in this limit, changes in F_{ν} cause a nonlinear response in F_{ν} . In the local limit when functional connectivity is driven by small-scale landscape structure, by contrast, reducing F_{ν} results in a nonlinear increase in functional connectivity. This is due to the linear correspondence between structural and functional connectivity metrics in this limit.

The simulations echo previous findings (Saco et al., 2020) that decreasing F_{ν} may produce a nonlinear increase in hydrologic connectivity for sparse vegetation cover. However, unlike these previous findings, the results do not identify threshold-like behavior between resource-capturing and resource-shedding modes of runoff behavior. Thus the breakpoint between high and low rainfall use efficiency observed by Saco et al. (2020) may reflect other factors, such as vegetation sensitivity to drought, or a piece-wise linear approximation of the geometric F_{ν} –FL nonlinearity (Rodríguez et al., 2018).

4.1. Practical implications for landscape assessment

The results point to a range of rainfall intensities for which flow-length provides a reliable indicator of functional connectivity at storm timescales. While this range depends on landscape and soil characteristics, FL most closely corresponds to both functional connectivity metrics in cases with rainfall intensities that generate runoff within bare soil areas $(p > K_b)$, but are significantly less than the hydraulic conductivity of vegetated patches $(p \ll K_v)$. By contrast, in settings where high-intensity storms dominate, the mean vegetation cover fraction may be a better indicator of functional connectivity.

The results show minor sensitivity to the slope angle for gentle slopes (see the comparison between So=0.5% and 5% in supporting Figure S9, where the 5% simulations display more global runoff behaviour in many but not all cases). The transition from local to global regimes may occur at lower storm intensities/durations on steeper hillslopes. However, the simulations were limited to gentle slopes to ensure that the Froude numbers remain subcritical at all locations (i.e., no hydraulic jumps are encountered). Moreover, on steeper slopes, it is

possible that processes related to flow concentration and erosion – processes omitted in this study – may cause topographic, rather than edaphic and vegetation-related controls to become the main determinants of connectivity. In this case, the flowlength metric may indicate the concentrated flow pathways established by previous storm events, which would provide a measure of topographic rather than bare soil connectivity. Thus, the robustness of flowlength as a measure of functional connectivity for steep hillslope gradients cannot be inferred from the present results.

The correspondence between flowlength and functional connectivity is also likely to be influenced by factors that we omitted in the present study for the purposes of simplicity. These factors include antecedent soil moisture (i.e., time-varying rates of infiltration, Liu et al., 2013; Mayor et al., 2019; Masselink et al., 2017), microtopography and surface roughness (Peñuela et al., 2016; Caviedes-Voullième et al., 2021), gradational transitions in infiltration rates between vegetation and interspace areas (Dunkerley, 2000; Madsen et al., 2008; Leite et al., 2020), and time-varying rainfall intensity (Dunkerley, 2021). While we did not explicitly evaluate these factors, their expected influence on the runoff regime can be outlined. For a given storm duration and intensity, Figs. 4 and 5 suggest that, particularly when the runoff regime is transitioning between 'local' and 'global' limits, vegetation patches that act as stronger runoff sinks (larger values of K_{ν}) promote more 'local' runoff behavior. Thus, omitted factors that increase the capacity of vegetation to absorb runoff are likely to improve the reliability of FL as a predictor of functional connectivity, and vice versa. For example, the assumption of steady infiltration (i.e., neglecting sorptivity effects), reduces the simulated infiltration rates relative to infiltration into dry soils. Important sorptivity effects would thus increase the infiltrability of the vegetation patches relative to bare soil areas, and thus the correspondence between flowlength and functional connectivity. Explicitly including a gradual transition between bare soil and vegetation - i.e., blurring the boundaries between bare soil and vegetation - is likely to weaken the predictive power of both FL and F_V .

The effects of microtopography likely depend on how effectively microtopography is accounted for when computing flowlength. Vegetation is often associated with microtopographic mounds (Bochet et al., 2000), which could serve to route runoff around vegetated areas. Soil mounding and greater infiltration rates under shrubs compete, with mounding impeding and infiltration enhancing run-on to vegetation. The effect of these interacting factors on how well flowlength represents functional connectivity is uncertain, even if soil mounds are accounted for in the flowlength computation. If microtopography is omitted in computing structural connectivity metrics, as it often must be in remote sensing assessments due to limited spatial resolution of data, then the computed flowlength may miss the tendency for microtopographic mounds to divert runoff around the vegetation. This would likely mean the role of vegetation as sinks was exaggerated, that the runoff regime would be more global than predicted initially, and structural and functional connectivity metrics diverge.

Finally, the insensitivity of C and L_{infl} to the spatial pattern identified in this study may not apply to specific patterns of vegetation distribution, for example when plants are preferentially clustered in one region of the hillslope, i.e., towards the bottom of the slope (Lapides et al., 2021), a feature observed in some dryland environments (Penny et al., 2013). Such clustering implies a degree of non-randomness in the vegetation cover distribution – whereas the study only considered random iso/anisotropic distributions – and evaluation of such non-randomness and its effects on connectivity is warranted in future work.

In light of the outstanding questions related to how the relation between structural and functional connectivity is impacted by rainfall variability, sorptivity effects, microtopography, transitions to concentrated flow, and non-random vegetation spatial patterns, more research is needed to design indicators for the assessment of landscape vegetation pattern (Carter et al., 2020; Carter et al., 2021).

4.2. Are both limits relevant to dryland ecohydrology?

Drylands clearly experience variations in rainfall climatology, topography and soil, which could produce a spectrum of local, global, and intermediate runoff regimes over time. Nevertheless, given that functional and structural connectivity metrics become decoupled in the global limit, it is important to understand whether all regimes are relevant to drylands.

Extensive research demonstrating links between the spatial pattern of vegetation and ecohydrological function in dryland systems suggests that the local limit is often relevant (Noy-Meir, 1979; Barbier et al., 2006; Saco and Moreno-de las Heras, 2013). At storm timescales, numerous field observations demonstrate that vegetation pattern governs runoff run-on behavior. For example, measures relating to the spatial organization of vegetation (i.e., patch size and landscape position) explain runoff and soil erosion better than the vegetation cover fraction alone (Puigdefábregas, 2005; Bautista et al., 2007; Arnau-Rosalén et al., 2008).

On longer timescales relevant to plant growth and dispersal, the formation of regular spatial patterns in drylands (e.g., banded formations on slope gradients and spotted or labyrinthine patterns on flat terrain, Barbier et al., 2006; Deblauwe et al., 2012) is hypothesized to arise through the redistribution of runoff from bare soil to vegetated patches (local facilitation) in combination with global water scarcity and nutrient limitation (Rietkerk et al., 2002; HilleRisLambers et al., 2001).

At both timescales, field evidence, therefore, suggests the importance of local runoff regimes for ecologic function in drylands.

However, before the conceptual framework of local and global runoff regimes can inform the interpretation of landscape indicators, two key limitations of the study need to be addressed: (i) the timescale separation between storm events and vegetation growth, and (ii) the assumption that the landscape structure is fixed on storm timescales.

Rainfall events occur on timescales of minutes to hours, while vegetation growth and dispersal occur on longer, annual to decadal timescales. The study results relate structural and functional connectivity metrics at storm timescales, for prescribed, randomly generated vegetation patterns. While the generated patterns span a large range of patch lengthscales and anisotropies, vegetation in reality grows, disperses and comes into equilibrium with its local climate over a large number of rainfall events. Future models that consider the co-evolution of structural and functional connectivity on much longer timescales may indicate some coordination between the two connectivity measures that is not fully explored in this study.

The assumption that structural connectivity is stationary at storm timescales may also not apply for extreme rainfall events. Mobilization and loss of sediment from the landscape under extreme rainfall conditions can modify preferential flow path, ultimately changing the structural aspects of connectivity, and subsequent behavior in the local limit (González-Hidalgo et al., 2007; Wainwright et al., 2011; Okin et al., 2015; Turnbull and Wainwright, 2019). Furthermore, the SVE model assumes sheet flow, and does not resolve preferential flow paths or concentrated flows (e.g., gullies) that may develop, particularly for larger storm events. While the simulation results characterize the conditions for which vegetation spatial pattern is a robust indicator for hydrologic connectivity, the rainfall conditions required to disturb landscape structure were not interrogated.

5. Conclusions

By mathematically simulating a broad range of rainfall and landscape conditions, two hydrologic 'end-member' limits have been identified. The first is a 'local' limit, in which functional connectivity can be approximated by structural connectivity. The second is a 'global' limit, in which vegetation fraction becomes a reliable indicator of hydrologic outcomes. In the local limit – corresponding to less intense, shorter

storms and more permeable soils in vegetation patches – both sourcesink and outlet connectivity are sensitive to the spatial configuration of the vegetation. In the global limit, by contrast, these metrics are well predicted by the hillslope vegetation cover fraction, but relatively insensitive to the spatial configuration of that vegetation. In both limits, functional connectivity is predictable: from structural connectivity in the local limit, and from vegetation cover fraction in the global limit (see Fig. 7). In identifying limiting behaviours, the study results help to clarify the conditions under which the nonlinear relation between vegetation cover fraction and structural connectivity (i.e., the flowlength index) extends to functional connectivity. Finally, the results offer guidance regarding the rainfall conditions for which structural connectivity (e.g., flowlength) is a reliable measure of functional connectivity, and can thus be implemented in dryland assessment. Further research is needed to characterize how other factors - including antecedent soil moisture - mediate relations between functional and structural connectivity.

Open Research

This manuscript relied only on model output generated by the authors during the course of the study. Version 1.09 of FullSWOF_2D used for the model simulations is available at DOI 10.21105/joss.00448 via CeCILL and developed openly at https://www.idpoisson.fr/fullswof/. The model simulation results used in the study are available at Open Science Foundation at https://osf.io/tnj2g/

Declaration of Competing Interest

The authors declare that they have no known competing financial interests or personal relationships that could have appeared to influence the work reported in this paper.

Data availability

Code and data shared on OSF

Acknowledgments

OC acknowledges funding from the National Science Foundation (NSF) Grant No. EAR-PF-1952651; GK acknowledges support from NSF-AGS-2028644, and the U.S. Department of Energy (DE-SC0022072); and DL acknowledges support from Simon Fraser University and USDA Forest Service Pacific Southwest Research Station, with funds administered by Oak Ridge Institute for Science and Education (ORISE).

Appendix A. Supplementary material

Supplementary data associated with this article can be found, in the online version, at https://doi.org/10.1016/j.catena.2023.107322.

References

- Anderies, J.M., Janssen, M.A., Walker, B.H., 2002. Grazing management, resilience, and the dynamics of a fire-driven rangeland system. Ecosystems 5, 23–44.
- Arnau-Rosalén, E., Calvo-Cases, A., Boix-Fayos, C., Lavee, H., Sarah, P., 2008. Analysis of soil surface component patterns affecting runoff generation. an example of methods applied to mediterranean hillslopes in alicante (spain). Geomorphology 101, 595–606.
- Assouline, S., 2004. Rainfall-induced soil surface sealing: A critical review of observations, conceptual models, and solutions. Vadose Zone J. 3, 570–591.
- Assouline, S., Thompson, S., Chen, L., Svoray, T., Sela, S., Katul, G., 2015. The dual role of soil crusts in desertification. J. Geophys. Res.: Biogeosci. 120, 2108–2119.
- Barbier, N., Couteron, P., Lejoly, J., Deblauwe, V., Lejeune, O., 2006. Self-organized vegetation patterning as a fingerprint of climate and human impact on semi-arid ecosystems. J. Ecol. 94, 537–547.
- Bautista, S., Mayor, A.G., Bourakhouadar, J., Bellot, J., 2007. Plant spatial pattern predicts hillslope runoff and erosion in a semiarid mediterranean landscape. Ecosystems 10, 987–998.

Belnap, J., 2006. The potential roles of biological soil crusts in dryland hydrologic cycles. Hydrol. Process.: An Int. J. 20, 3159–3178.

- Bochet, E., Poesen, J., Rubio, J.L., 2000. Mound development as an interaction of individual plants with soil, water erosion and sedimentation processes on slopes. Earth Surface Process. Landforms: J. Brit. Geomorphol. Res. Group 25, 847–867.
- Bracken, L., Wainwright, J., Ali, G., Tetzlaff, D., Smith, M., Reaney, S., Roy, A., 2013. Concepts of hydrological connectivity: Research approaches, pathways and future agendas. Earth Sci. Rev. 119, 17–34.
- Bracken, L.J., Croke, J., 2007. The concept of hydrological connectivity and its contribution to understanding runoff-dominated geomorphic systems. Hydrol. Process.: An Int. J. 21, 1749–1763.
- Brutsaert, W., 2005. Hydrology: an introduction. Cambridge University Press. Cammeraat, E.L., 2004. Scale dependent thresholds in hydrological and erosion response of a semi-arid catchment in southeast Spain. Agric., Ecosyst. Environ. 104, 317–332.
- Cantón, Y., Solé-Benet, A., De Vente, J., Boix-Fayos, C., Calvo-Cases, A., Asensio, C., Puigdefábregas, J., 2011. A review of runoff generation and soil erosion across scales in semiarid south-eastern spain. J. Arid Environ. 75, 1254–1261.
- Carter, S.K., Burris, L., Domschke, C.T., Garman, S.L., Haby, T., Harms, B.R., Kachergis, E., Litschert, S., Miller, K.H., 2021. Identifying policy-relevant indicators for assessing landscape vegetation patterns to inform planning and management on multiple-use public lands. Environmental management 68, 426–443.
- Carter, S.K., Pilliod, D.S., Haby, T., Prentice, K.L., Aldridge, C.L., Anderson, P.J., Bowen, Z.H., Bradford, J.B., Cushman, S.A., DeVivo, J.C., et al., 2020. Bridging the research-management gap: landscape science in practice on public lands in the western united states. Landscape Ecol. 35, 545–560.
- Caviedes-Voullième, D., Ahmadinia, E., Hinz, C., 2021. Interactions of microtopography, slope and infiltration cause complex rainfall-runoff behavior at the hillslope scale for single rainfall events. Water resources research 57 e2020WR028127.
- Cheng, N.-S., Nguyen, H.T., 2011. Hydraulic radius for evaluating resistance induced by simulated emergent vegetation in open-channel flows. J. Hydraul. Eng. 137, 995–1004.
- Crompton, O., Sytsma, A., Thompson, S., 2019. Emulation of the saint venant equations enables rapid and accurate predictions of infiltration and overland flow velocity on spatially heterogeneous surfaces. Water Resour. Res. 55, 7108–7129.
- Deblauwe, V., Couteron, P., Bogaert, J., Barbier, N., 2012. Determinants and dynamics of banded vegetation pattern migration in arid climates. Ecol. Monogr. 82, 3–21.
- Delestre, O., Cordier, S., Darboux, F., Du, M., James, F., Laguerre, C., Lucas, C., Planchon, O., 2014. Fullswof: A software for overland flow simulation. In: Advances in hydroinformatics. Springer, pp. 221–231.
- D'Odorico, P., Laio, F., Ridolfi, L., 2006. Patterns as indicators of productivity enhancement by facilitation and competition in dryland vegetation. Journal of Geophysical Research. Biogeosciences 111.
- Dunkerley, D., 2021. Rainfall intensity in geomorphology: Challenges and opportunities. Prog. Phys. Geogr.: Earth Environ. 45, 488–513.
- Dunkerley, D.L., 2000. Assessing the influence of shrubs and their interspaces on enhancing infiltration in an arid australian shrubland. Rangeland J. 22, 58–71.
- Dunkerley, D.L., 2002. Infiltration rates and soil moisture in a groved mulga community near alice springs, arid central australia: evidence for complex internal rainwater redistribution in a runoff–runon landscape. J. Arid Environ. 51, 199–219.
- Dunkerley, D.L., 2003. Determining friction coefficients for interrill flows: the significance of flow filaments and backwater effects. Earth Surf. Process. Landforms: J. Brit. Geomorphol. Res. Group 28, 475–491.
- Fatichi, S., Vivoni, E.R., Ogden, F.L., Ivanov, V.Y., Mirus, B., Gochis, D., Downer, C.W., Camporese, M., Davison, J.H., Ebel, B., et al., 2016. An overview of current applications, challenges, and future trends in distributed process-based models in hydrology. J. Hydrol. 537, 45–60.
- Gao, Y., Zhong, B., Yue, H., Wu, B., Cao, S., 2011. A degradation threshold for irreversible loss of soil productivity: a long-term case study in china. J. Appl. Ecol. 48, 1145–1154.
- Garcia-Estringana, P., Alonso-Blázquez, N., Marques, M., Bienes, R., Alegre, J., 2010. Direct and indirect effects of mediterranean vegetation on runoff and soil loss. Eur. J. Soil Sci. 61, 174–185.
- Gibbens, R., McNeely, R., Havstad, K., Beck, R., Nolen, B., 2005. Vegetation changes in the jornada basin from 1858 to 1998. J. Arid Environ. 61, 651–668.
- González-Hidalgo, J.C., Peña-Monné, J.L., de Luis, M., 2007. A review of daily soil erosion in western mediterranean areas. Catena 71, 193–199.
- Harman, C.J., Lohse, K.A., Troch, P.A., Sivapalan, M., 2014. Spatial patterns of vegetation, soils, and microtopography from terrestrial laser scanning on two semiarid hillslopes of contrasting lithology. Journal of Geophysical Research: Biogeosciences 119, 163–180.
- HilleRisLambers, R., Rietkerk, M., van den Bosch, F., Prins, H.H., de Kroon, H., 2001.Vegetation pattern formation in semi-arid grazing systems. Ecology 82, 50–61.
- Imeson, A., Prinsen, H., 2004. Vegetation patterns as biological indicators for identifying runoff and sediment source and sink areas for semi-arid landscapes in spain. Agriculture, ecosystems & environment 104, 333–342.
- James, C., Birkhead, A., Jordanova, A., O'sullivan, J., 2004. Flow resistance of emergent vegetation. J. Hydraul. Res. 42, 390–398.
- Kéfi, S., Rietkerk, M., Alados, C.L., Pueyo, Y., Papanastasis, V.P., ElAich, A., De Ruiter, P. C., 2007. Spatial vegetation patterns and imminent desertification in mediterranean arid ecosystems. Nature 449, 213–217.
- Kéfi, S., Saade, C., Berlow, E.L., Cabral, J.S., Fronhofer, E.A., 2022. Scaling up our understanding of tipping points. Philosophical Transactions of the Royal Society B 377, 20210386.
- Kirstetter, G., Hu, J., Delestre, O., Darboux, F., Lagrée, P.-Y., Popinet, S., Fullana, J.-M., Josserand, C., 2016. Modeling rain-driven overland flow: Empirical versus analytical friction terms in the shallow water approximation. J. Hydrol. 536, 1–9.

- Lapides, D.A., Leclerc, C.D., Moidu, H., Dralle, D.N., Hahm, W.J., 2021. Variability of stream extents controlled by flow regime and network hydraulic scaling. Hydrol. Process. 35, e14079.
- Leite, P.A., Wilcox, B.P., McInnes, K.J., 2020. Woody plant encroachment enhances soil infiltrability of a semiarid karst savanna. Environmental Research Communications 2, 115005.
- Li, H., Reynolds, J.F., 1994. A simulation experiment to quantify spatial heterogeneity in categorical maps. Ecology 75, 2446–2455.
- Liu, Y., Fu, B., Lü, Y., Gao, G., Wang, S., Zhou, J., 2013. Linking vegetation cover patterns to hydrological responses using two process-based pattern indices at the plot scale. Science China Earth Sciences 56, 1888–1898.
- Ludwig, J., Tongway, D., Hodgkinson, K., Freudenberger, D., Noble, J., 1996. Landscape ecology, function and management: principles from Australia's rangelands. Csiro Publishing.
- Ludwig, J.A., Bartley, R., Hawdon, A.A., Abbott, B.N., McJannet, D., 2007a. Patch configuration non-linearly affects sediment loss across scales in a grazed catchment in north-east australia. Ecosystems 10, 839–845.
- Ludwig, J.A., Bastin, G.N., Chewings, V.H., Eager, R.W., Liedloff, A.C., 2007b. Leakiness: a new index for monitoring the health of arid and semiarid landscapes using remotely sensed vegetation cover and elevation data. Ecol. Ind. 7, 442–454.
- Ludwig, J.A., Eager, R.W., Bastin, G.N., Chewings, V.H., Liedloff, A.C., 2002. A leakiness index for assessing landscape function using remote sensing. Landscape ecology 17, 157–171.
- Madsen, M., Chandler, D., Belnap, J., 2008. Spatial gradients in ecohydrologic properties within a pinyon-juniper ecosystem. Ecohydrology: Ecosystems. Land and Water Process Interactions, Ecohydrogeomorphology 1, 349–360.
- Maestre, F.T., Salguero-Gomez, R., & Quero, J.L. (2012). It is getting hotter in here: determining and projecting the impacts of global environmental change on drylands.
- Magliano, P.N., Breshears, D.D., Fernández, R.J., Jobbágy, E.G., 2015. Rainfall intensity switches ecohydrological runoff/runon redistribution patterns in dryland vegetation patches. Ecological applications 25, 2094–2100.
- Mander, L., Dekker, S.C., Li, M., Mio, W., Punyasena, S.W., Lenton, T.M., 2017.
 A morphometric analysis of vegetation patterns in dryland ecosystems. Royal Society open science 4, 160443.
- Masselink, R.J., Heckmann, T., Temme, A.J., Anders, N.S., Gooren, H.P., Keesstra, S.D., 2017. A network theory approach for a better understanding of overland flow connectivity. Hydrol. Process. 31, 207–220.
- Mayor, A.G., Bautista, S., Bellot, J., 2009. Factors and interactions controlling infiltration, runoff, and soil loss at the microscale in a patchy mediterranean semiarid landscape. Earth Surf. Proc. Land. 34, 1702–1711.
- Mayor, A.G., Bautista, S., Rodriguez, F., Kéfi, S., 2019. Connectivity-mediated ecohydrological feedbacks and regime shifts in drylands. Ecosystems 22, 1497–1511.
- Mayor, A.G., Bautista, S., Small, E.E., Dixon, M., Bellot, J., 2008. Measurement of the connectivity of runoff source areas as determined by vegetation pattern and topography: A tool for assessing potential water and soil losses in drylands. Water Resour. Res. 44.
- Moreno-De-Las-Heras, M., Merino-Martín, L., Saco, P.M., Espigares, T., Gallart, F., Nicolau, J.M., 2020. Structural and functional control of surface-patch to hillslope runoff and sediment connectivity in mediterranean dry reclaimed slope systems. Hydrol. Earth Syst. Sci. 24, 2855–2872.
- Mügler, C., Ribolzi, O., Janeau, J.-L., Rochelle-Newall, E., Latsachack, K., Thammahacksa, C., Viguier, M., Jardé, E., Henri-Des-Tureaux, T., Sengtaheuanghoung, O., et al., 2019. Experimental and modelling evidence of short-term effect of raindrop impact on hydraulic conductivity and overland flow intensity. J. Hydrol. 570. 401–410.
- Muñoz-Robles, C., Tighe, M., Reid, N., Frazier, P., Briggs, S.V., Wilson, B., 2013. A twostep up-scaling method for mapping runoff and sediment production from pasture and woody encroachment on semi-arid hillslopes. Ecohydrology 6, 83–93.
- Noy-Meir, I., 1979. Structure and function of desert ecosystems. Israel Journal of Plant Sciences 28, 1–19.
- Okin, G.S., Heras, M.M.-d. I., Saco, P.M., Throop, H.L., Vivoni, E.R., Parsons, A.J., Wainwright, J., Peters, D.P., 2015. Connectivity in dryland landscapes: shifting concepts of spatial interactions. Front. Ecol. Environ. 13, 20–27.
- Okin, G.S., Parsons, A.J., Wainwright, J., Herrick, J.E., Bestelmeyer, B.T., Peters, D.C., Fredrickson, E.L., 2009. Do changes in connectivity explain desertification? Bioscience 59, 237–244.
- Penny, G.G., Daniels, K.E., Thompson, S.E., 2013. Local properties of patterned vegetation: quantifying endogenous and exogenous effects. Philosophical Transactions of the Royal Society A: Mathematical, Physical and Engineering Sciences 371, 20120359.

Peñuela, A., Darboux, F., Javaux, M., Bielders, C.L., 2016. Evolution of overland flow connectivity in bare agricultural plots. Earth Surf. Proc. Land. 41, 1595–1613.

- Puigdefábregas, J., 2005. The role of vegetation patterns in structuring runoff and sediment fluxes in drylands. Earth Surface Processes and Landforms: The Journal of the British Geomorphological Research Group 30, 133–147.
- Reaney, S., Bracken, L.J., Kirkby, M., 2014. The importance of surface controls on overland flow connectivity in semi-arid environments: Results from a numerical experimental approach. Hydrol. Process. 28, 2116–2128.
- Reynolds, J.F., Smith, D.M.S., Lambin, E.F., Turner, B., Mortimore, M., Batterbury, S.P., Downing, T.E., Dowlatabadi, H., Fernández, R.J., Herrick, J.E., et al., 2007. Global desertification: building a science for dryland development. Science 316, 847–851.
- Rietkerk, M., Boerlijst, M.C., van Langevelde, F., HilleRisLambers, R., de Koppel, J.v., Kumar, L., Prins, H.H., de Roos, A.M., 2002. Self-organization of vegetation in arid ecosystems. Am. Nat. 160, 524–530.
- Rodríguez, F., Mayor, A.G., Rietkerk, M., Bautista, S., 2018. A null model for assessing the cover-independent role of bare soil connectivity as indicator of dryland functioning and dynamics. Ecol. Ind. 94, 512–519.
- Rodríguez-Caballero, E., Cantón, Y., Lazaro, R., Solé-Benet, A., 2014. Cross-scale interactions between surface components and rainfall properties. non-linearities in the hydrological and erosive behavior of semiarid catchments. J. Hydrol. 517,
- Saco, P.M., Moreno-de las Heras, M., 2013. Ecogeomorphic coevolution of semiarid hillslopes: Emergence of banded and striped vegetation patterns through interaction of biotic and abiotic processes. Water Resour. Res. 49, 115–126.
- Saco, P.M., Rodríguez, J.F., Moreno-de las Heras, M., Keesstra, S., Azadi, S., Sandi, S., Baartman, J., Rodrígo-Comino, J., Rossi, M.J., 2020. Using hydrological connectivity to detect transitions and degradation thresholds: Applications to dryland systems. Catena 186. 104354.
- Schlesinger, W.H., Reynolds, J.F., Cunningham, G.L., Huenneke, L.F., Jarrell, W.M., Virginia, R.A., Whitford, W.G., 1990. Biological feedbacks in global desertification. Science 247, 1043–1048.
- Schumaker, N.H., 1996. Using landscape indices to predict habitat connectivity. Ecology 77, 1210–1225.
- Šimunek, J., Angulo-Jaramillo, R., Schaap, M.G., Vandervaere, J.-P., van Genuchten, M. T., 1998. Using an inverse method to estimate the hydraulic properties of crusted soils from tension-disc infiltrometer data. Geoderma 86, 61–81.
- Smith, M.W., Cox, N.J., Bracken, L.J., 2007. Applying flow resistance equations to overland flows. Prog. Phys. Geogr. 31, 363–387.
- Thompson, S., Harman, C., Heine, P., Katul, G., 2010a. Vegetation-infiltration relationships across climatic and soil type gradients. Journal of Geophysical Research. Biogeosciences 115.
- Thompson, S., Katul, G., 2011. Inferring ecosystem parameters from observation of vegetation patterns. Geophys. Res. Lett. 38.
- Thompson, S., Katul, G., Konings, A., Ridolfi, L., 2011. Unsteady overland flow on flat surfaces induced by spatial permeability contrasts. Advances in water resources 34, 1049–1058.
- Thompson, S.E., Assouline, S., Chen, L., Trahktenbrot, A., Svoray, T., Katul, G.G., 2014. Secondary dispersal driven by overland flow in drylands: Review and mechanistic model development. Movement ecology 2, 1–13.
- Thompson, S.E., Katul, G.G., Porporato, A., 2010b. Role of microtopography in rainfall-runoff partitioning: An analysis using idealized geometry. Water Resour. Res. 46.
- Turnbull, L., Wainwright, J., 2019. From structure to function: Understanding shrub encroachment in drylands using hydrological and sediment connectivity. Ecol. Ind. 98, 608–618.
- Turnbull, L., Wainwright, J., Brazier, R.E., 2008. A conceptual framework for understanding semi-arid land degradation: Ecohydrological interactions across multiple-space and time scales. Ecohydrology: Ecosystems, Land and Water Process Interactions, Ecohydrogeomorphology 1, 23–34.
- Valentin, C., Casenave, A., 1992. Infiltration into sealed soils as influenced by gravel cover. Soil Sci. Soc. Am. J. 56, 1667–1673.
- Vásquez-Méndez, R., Ventura-Ramos, E., Oleschko, K., Hernández-Sandoval, L., Parrot, J.-F., Nearing, M.A., 2010. Soil erosion and runoff in different vegetation patches from semiarid central mexico. Catena 80, 162–169.
- Wainwright, J., Turnbull, L., Ibrahim, T.G., Lexartza-Artza, I., Thornton, S.F., Brazier, R. E., 2011. Linking environmental regimes, space and time: Interpretations of structural and functional connectivity. Geomorphology 126, 387–404.
- Wu, G., Shu, L., Lu, C., Chen, X., 2016. The heterogeneity of 3-d vertical hydraulic conductivity in a streambed. Hydrol. Res. 47, 15–26.